Available online at www.sciencedirect.com

SCIENCE DIRECT®

Tectonophysics 408 (2005) 213–236

TECTONOPHYSICS

www.elsevier.com/locate/tecto

Late Quaternary activity of the Pajarito fault, Rio Grande rift of northern New Mexico, USA

James P. McCalpin *

GEO-HAZ Consulting, Inc., P.O. Box 837, Crestone, CO 81131, USA

Received 15 April 2003; accepted 31 May 2005
Available online 1 September 2005

Abstract

The Pajarito fault forms the western margin of the Rio Grande rift in north-central New Mexico, and lies adjacent to Los Alamos National Laboratory, a major Federal research facility. Vertical displacement on this normal fault over the past 1.2 Ma has created a 50- to 120-m-high fault scarp on Bandelier Tuff (1.2 Ma), yielding a long-term average slip rate of ca. 0.1 mm/yr. In support of a Laboratory-wide seismic hazards assessment, we excavated 14 trenches in the Pajarito fault zone to determine the age of the most recent displacement event, the recurrence interval between events, the displacement per event, and the variability in slip rate and recurrence through time. The large number of trenches was required by the large height of the fault scarp and the complexity of the fault zone. Only about half the trenches contained significant thicknesses of Holocene deposits, but in those trenches there was clear evidence for an early-to-mid-Holocene displacement event. The previous event was at least 20–40 ka, and the average recurrence interval over the past ca. 300 ka was about 20–40 kyr. We infer that much of the structural relief across this fault developed soon after eruption of the Bandelier Tuff between 1.0 and 1.2 Ma, and that slip rate slowed considerably after that time.

Keywords: Paleoseismology; Quaternary faulting; Seismic hazard; Rio Grande rift

1. Introduction

The primary purpose of this trenching study was to date late Quaternary faulting events on the main trace of the Pajarito fault, particularly adjacent to Los Alamos National Laboratory (LANL). The Pajarito fault is an east-dipping normal fault that forms the western margin of the Rio Grande rift (Fig. 1) and is the master fault of a west-tilted half-graben occupied by the Española Basin (Kelley, 1978; Aldrich and Dethier, 1990). The Pajarito fault forms a 100- to 150-m-high, east-facing fault escarpment that separates the Jemez Mountains on the west from the Pajarito Plateau on the east (Fig. 2). The Jemez Mountains are cored by late Tertiary to early Quaternary andesitic and dacitic flows and caldera-derived

* Fax: +1 719 256 5228.
E-mail address: mccalpin@geohaz.com.

0040-1951
doi:10.1016/j.tecto.2005.05.038

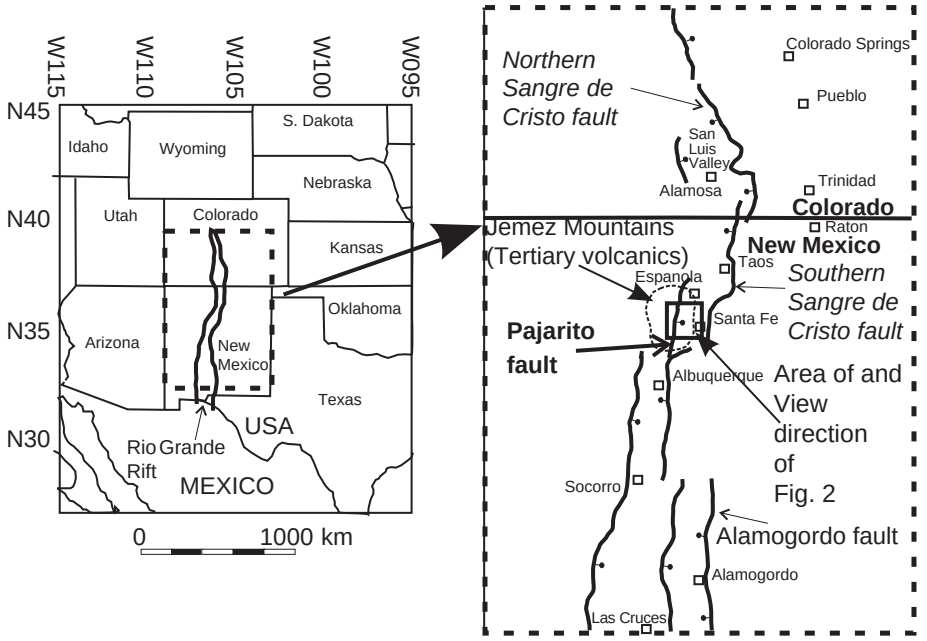

Fig. 1. Location map of Pajarito fault system. Left: location of the Rio Grande rift (thick black lines) in the southwestern United States. Right: detail of the Rio Grande rift in vicinity of northern New Mexico and southern Colorado. Thick black lines show major rift-bounding faults, with bar-and-ball on downthrown side.

tephras (Bailey et al., 1969; Smith et al., 1970; Gardner et al., 1986). The latest convulsive eruption there at 1.2 Ma formed the Valles Caldera and spread a wide blanket of ash-flow tuff as much as 100 m thick (Bandelier Tuff, Smith and Bailey, 1966). In the past 1.2 Ma, the Rio Grande flowing south down the rift axis has incised about 150 m below the tuff and has thus preserved the tuff-mantled Pajarito Plateau west of the river. Los Alamos National Laboratory, a large Federal research complex, is located on the relatively undissected western part of the Plateau, at the foot of the Pajarito fault escarpment and Jemez Mountains. The eastern part of the Pajarito Plateau is dissected by numerous east-flowing drainages that deepen eastward to reach the incised channel of the Rio Grande (Fig. 2).

Previous studies of seismic hazards to the National Laboratory have yielded relatively well-constrained ages for the latest faulting events on two subsidiary antithetic faults, the Rendija Canyon fault (RCF) and Guaje Mountain fault (GMF) (Gardner et al., 1990; Wong et al., 1993, 1995; Olig et al., 1996; Kelson et al., 1996), but sparse information was derived from the master Pajarito fault (PF) of the Pajarito fault zone (PFZ). On the RCF, the most recent event (MRE) was dated at either 8 ka (based on radiocarbon) or 23 ka (based on luminescence; Kelson et al., 1996). On the GMF, the MRE was dated at 4–6 ka (Gardner et al., 1990). In contrast, trenches along the base of the "master" Parajito fault (PF) indicate that the youngest dated faulting event was dated as older than ca. 50–60 ka according to Wong et al. (1995) and Olig et al. (1996). Thus, the Holocene (or late Pleistocene) surface faulting events on the smaller, antithetic RCF and GMF apparently were not accompanied by surface faulting on the larger, master Pajarito normal fault. This anomalous situation demanded a more detailed paleoseismic study of the master (PF) fault.

The primary goal of this study was to identify and date the latest several faulting events on the Pajarito fault. The secondary purpose of trenching was to refine estimates for displacement per event, slip rate, and recurrence intervals for faulting events on the fault. Values for these seismic source parameters derived from previous trenches (Wong et al., 1995)

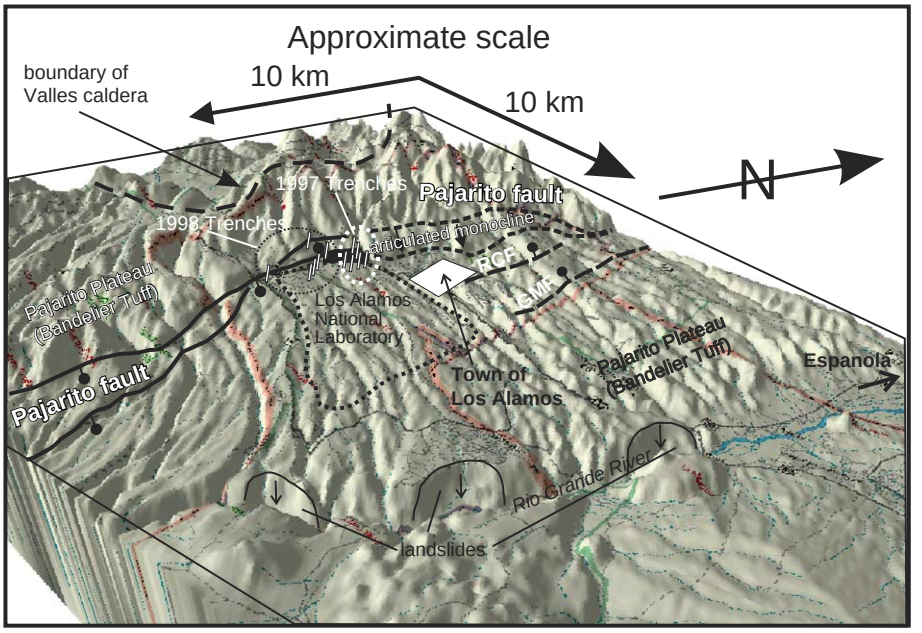

Fig. 2. Perspective shaded relief Digital Elevation Model of the dissected, 1.2 Ma Pajarito Plateau (middle ground), the Pajarito fault zone at the western margin of the Plateau (thick black lines, bar-and-ball on downthrown side), and the Valles Caldera of the Jemez Mountains (upper left), looking northwest. Directly west of Los Alamos National Laboratory the Pajarito fault zone consists of two scarps, an eastern 100-m-high main scarp and a western 30-m-high splay scarp (located at the right end of the label "1998 trenches"). All trenches described in this report were in the main fault zone, except for Trench 98-4 which was on the western splay scarp. The incised valley of the Rio Grande lies in the foreground; river flows from right to left.

were poorly constrained because none of those trenches captured a complete paleoearthquake sequence for the relatively wide scarp of the PF.

1.1. Structural style of the Pajarito fault and trenching strategy

The Pajarito fault is expressed as a complex, 50- to 150-m-high escarpment on welded and nonwelded tuff (Fig. 3). The escarpment is thus more like a small incipient range front, than a fault scarp developed on unconsolidated Quaternary deposits, for which most paleoseismic trenching techniques were developed. In 1996, I mapped the PF scarp at a scale of 1 : 1200 (McCalpin, 1997) and determined that the 8 km of scarp adjacent to LANL consisted of an "articulated" or "segmented" monocline (about 50% of its length), landslide blocks (about 30% of its length), and a simple high-angle normal fault (about 20% of its length). However, there were also parts of the escarpment composed of multiple, synthetic step faults. Based on the detailed mapping, all four structure types identified by Powell (1873) for faulted monoclines in the Colorado Plateau were present (Fig. 4) and graded laterally into each other.

The Pajarito fault zone reaches its greatest width (ca. 2 km) directly south of Los Alamos Canyon (Fig. 5). Here the main scarp is only about 50 m high and is the surface expression of an "articulated monocline", that is, a monocline composed of an east-tilted slab of welded tuff flanked by a large tension fissure at the scarp crest, and a graben at the scarp toe (Fig. 6). Over most of its length, the main PF scarp is underlain by east-tilted blocks of Bandelier Tuff, such that the scarp face is essentially a dip slope. These tuff blocks dip 30°–45° east and are separated from subhorizontal tuff above (west of) the scarp by large tension fissures. At the base of the main scarp there is typically a poorly exposed zone of normal faults, termed the basal fault zone. In some areas this basal fault zone forms the western boundary of a graben, the eastern boundary of which is one or more west-facing fault scarps. The east-tilted tuff blocks that form the scarp face may also be broken by mid-scarp tension fissures. About 8

Fig. 3. Photograph of the main scarp of the Pajarito fault zone in the area of the 1998 trenches, looking south. In distance, fault scarp (between black arrows) trends southeast; in foreground, main scarp (between white arrows) is 100 m high. Buildings at left center are part of Los Alamos National Laboratory.

km south of Los Alamos Canyon (where New Mexico Highway 4 ascends the scarp), road-cuts show that the scarp is underlain of many narrow fault-bounded blocks of tuff, 5–10 m wide, that have toppled up to 45° eastward; this geometry resembles that shown in Fig. 4d.

Given the complex structure and the large width and height of the main fault scarp, three possible

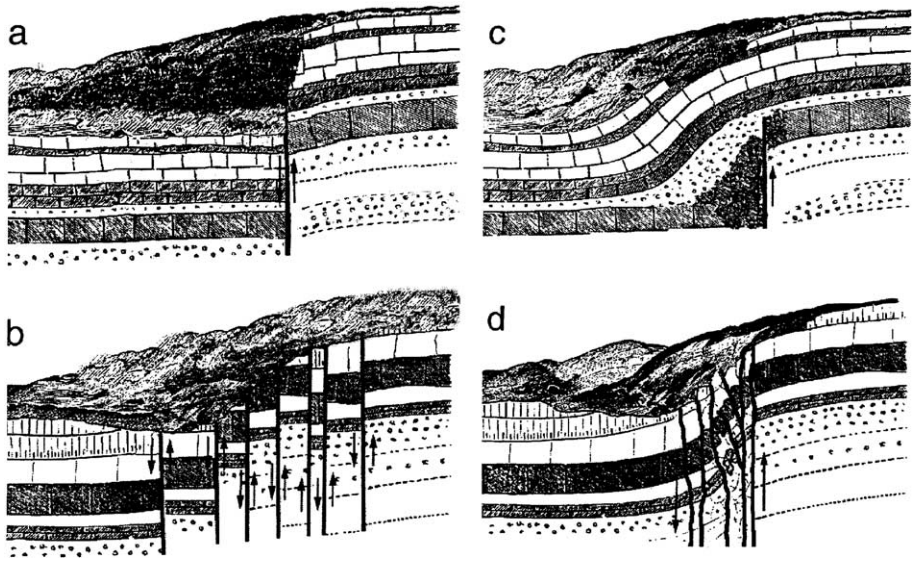

Fig. 4. Schematic cross-sections showing several styles of near-surface deformation on a normal fault zone in horizontally layered rocks, from examples on the Colorado Plateau of western United States. In these examples, from Powell (1873), the topographic escarpments are several hundred meters high. (a) Simple normal fault with prominent scarp; (b) broad zone of small normal faults (step faults); (c) monocline with normal fault at depth; (d) faulted monocline; fault-bounded blocks may be rotated (toppled) toward the downthrown block. The Pajarito fault zone exhibits each of these styles along strike, but in style c (monocline) the limb of the monocline is planar rather than curved and is bounded by a tension fissure on its up-slope side and by a normal fault (basal normal fault) on its down-slope side (cf. Fig. 6).

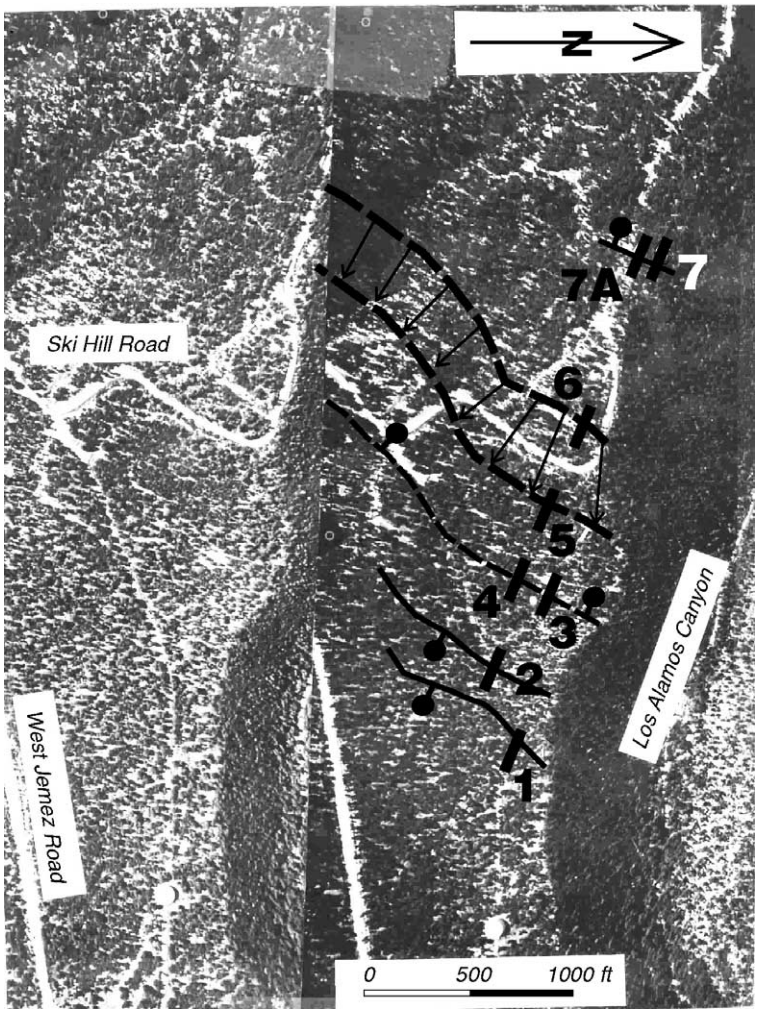

Fig. 5. Steropair of aerial photographs showing the transect of 7 trenches directly south of Los Alamos Canyon (the deep canyon at right) described in this paper. North is to the right. The ground surface here is everywhere underlain by the top of the 1.2 Ma Bandelier Tuff.

trenching strategies were envisioned. The first was a "megatrench" through the ca. 50-m-thick (?) colluvial wedge at the scarp base where the scarp was underlain by one or more high-angle normal faults (e.g., the geometry shown in Fig. 4a). This option was given low priority due to logistical problems of trenching through the thick colluvium. The second strategy consisted of multiple trenches scattered along strike on the PF scarp, but each on different structures. Although this strategy was logistically feasible, rupture events (including the MRE) might be missed due to the scattered locations of trenches. The third strategy, which we executed in 1997, involved a transect of eight trenches across all major component scarps of the PF at a given latitude. This strategy was considered the best for capturing evidence of the MRE on the Pajarito fault, which had so far eluded researchers. Our eight trenches (97-1 through 97-7A) were placed on the six major faults in this zone. A seventh deformation zone, the mid-scarp tension fissure, had mainly been destroyed by construction of Ski Hill Road (Fig. 5). In 1998 we excavated an additional six trenches at locations scattered along the Pajarito fault zone between Los Alamos Canyon and New Mexico Highway 4, including one trench on the western splay scarp (Trench 98-4, described later).

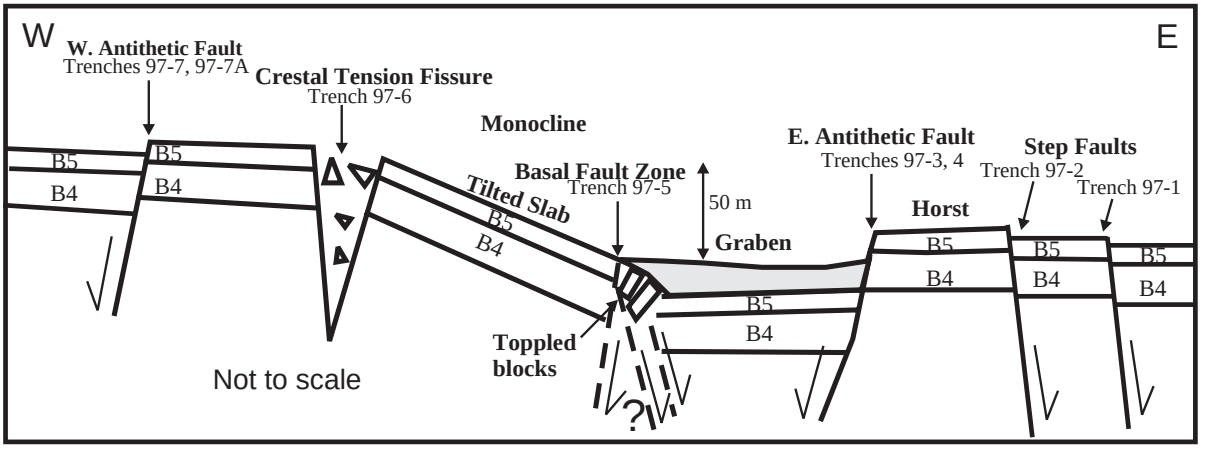

Fig. 6. Schematic cross-section through the Pajarito fault zone directly south of Los Alamos Canyon. The major geomorphic features of the fault zone at this latitude are: a western antithetic fault (Trenches 97-7, 97-7A), crestal tension fissure (Trench 97-6), east-tilted slab of the articulated monocline, basal fault zone (fault queried; Trench 97-5), 200-m-wide graben, antithetic fault on the eastern margin of the graben (Trenches 97-3, 97-4), a horst, and two synthetic step faults east of the graben (Trenches 97-1, 97-2). B5 and B4 indicate separate cooling units in the 1.2 Ma Bandelier Tuff. Shaded area in graben represents post-1.2 Ma graben-fill sediments (alluvium and colluvium).

1.2. Field methods

Fourteen trenches were excavated in structural depressions within the fault zone (graben, tension fissures, colluvial toeslopes) where unconsolidated, post-Bandelier Tuff sediment had accumulated (except Trenches 97-1 and 97-2, which were in Bandelier Tuff). These depressions were chosen because (1) the backhoe excavators could more easily dig through unconsolidated sediment than through the welded tuff, and (2) these sediment traps held the greatest potential for preserving episodic, fault-related deposits such as colluvial wedges (McCalpin, 1996). In most trenches, the unconsolidated sediment was locally derived colluvium composed of poorly sorted, poorly stratified gravelly sand. However, almost all the unconsolidated deposits were strongly affected by soil development manifested as reddish, clay-rich textural B horizons with as much as 40% clay. Therefore, in most of the 14 trenches logged the most obvious mappable contacts were soil horizon boundaries rather than stratigraphic contacts. In addition to our mapping of soil horizons, McDonald (1999) described vertical soil profiles at 11 locations in our trenches. He calculated Profile Development Index (PDI) for the soils and Soil Development Index (SDI) values for all horizons, after the methods of Harden (1982), Harden and Taylor (1983) and Taylor (1988); he then estimated the time required for soils to develop from independently dated SDI chronofunctions.

This paper mainly describes trenches dug in 1997 in the 8-trench transect across the entire width of the PF south of Los Alamos Canyon. First I describe 6 of the 8 trenches on the main scarp of the PF, including the basal fault zone (Trench 97-5), the graben antithetic scarp (Trenches 97-3, 97-4), the crestal tension fissure (Trench 97-6), and an antithetic fault on the footwall (Trenches 97-7, 97-7A). Trenches 97-1 and 97-2 across synthetic faults of the hanging wall exposed too thin a section of unconsolidated deposits to yield good paleoseismic data, and are not described herein. Second, I describe one of the two trenches excavated across the 30-m-high, 2 km-long "western splay scarp" that lies on the footwall of the main, 100-m-high PF scarp.

2. Trenches in the main scarp zone

2.1. Main scarp (Trench 97-5)

Trench 97-5 is located at the base of the main, 50-m-high scarp of the Pajarito fault south of Los Alamos Canyon, and exposes the basal fault zone (Figs. 5 and 6). The trench is 30 m long and up to 6.5 m deep (Fig. 7). The upslope end of the trench

Fig. 7. Photograph of Trench 97-5 at the base of the main, 50-m-high Pajarito fault scarp, looking west. The western (far) end of the trench is excavated into the down-slope, eastern tip of the forward-tilted slab of the articulated monocline.

coincides with the down-dip (eastern) end of the east-tilted slab of Bandelier Tuff that forms the scarp.

The trench exposes a series of six buried paleosols that dip east approximately parallel to the modern ground surface (Fig. 8, paleosols indicated by "b1" to "b6" at the end of the trench unit abbreviation). The paleosols are developed on sandy–silty slope wash that contains rare angular blocks of Bandelier Tuff. Near the head of the trench a series of east-dipping normal faults displace the paleosols by a few decimeters to more than 1 m. The two westernmost normal faults bound a block of Bandelier Tuff that protrudes up into the trench floor (Fig. 8, inset). Farther west is a large infilled tension fissure (Fig. 8, cross-hatched pattern), and then the overhanging tip of the monoclinal slab of tuff. Bandelier Tuff is faulted downward across the fault zone by an amount greater than trench depth.

Each of the paleosols represents a long (tens of kyr) period of slope stability and soil formation. McDonald (1999) estimated the age of the top of each soil from the cumulative SDI values combined with a calibrated relationship of SDI to numerical ages.

2.1.1. Paleoseismic interpretation

Four or five displacement events can be inferred from angular unconformities, stone lines, and fissure fills in Trench 97-5 (Fig. 8). Numerical age control comes from luminescence age estimates (Table 1), radiocarbon dates (Table 2), and SDI age estimates. If each of the seven soils represents a faulting event (rather than a climatic response), there have been seven such events in 492 ka. The latest 3 to 4 events post-date buried soil 3 (units 5Btb3, 5BCb3) have evidently occurred in the past ca. 177–184 ka (the SDI age for buried soil 3). By comparison, the retrodeformation sequence of Trench 97-3 on the opposite side of the graben (described later) requires six events (two of which had negligible net vertical displacement) in the past 110 ka. It seems reasonable that the main scarp (Trench 97-5) should record as many displacement events as the antithetic scarp (Trench 97-3), so we may have missed evidence of several events in Trench 97-5. For example, small-displacement events may not have formed stone lines because no free faces in tuff were created. Alternatively, small-displacement events may have created only small fissures that were engulfed by later larger fissures and made unrecognizable. Because this trench lacks significant coarse (debris-facies) scarp-derived colluvium, it appears that surface rupture does not form typical large, subvertical free faces in the basal fault zone, but rather, meter-scale normal faulting at depth is expressed as a combination of complex fissure opening and small-scale normal faulting.

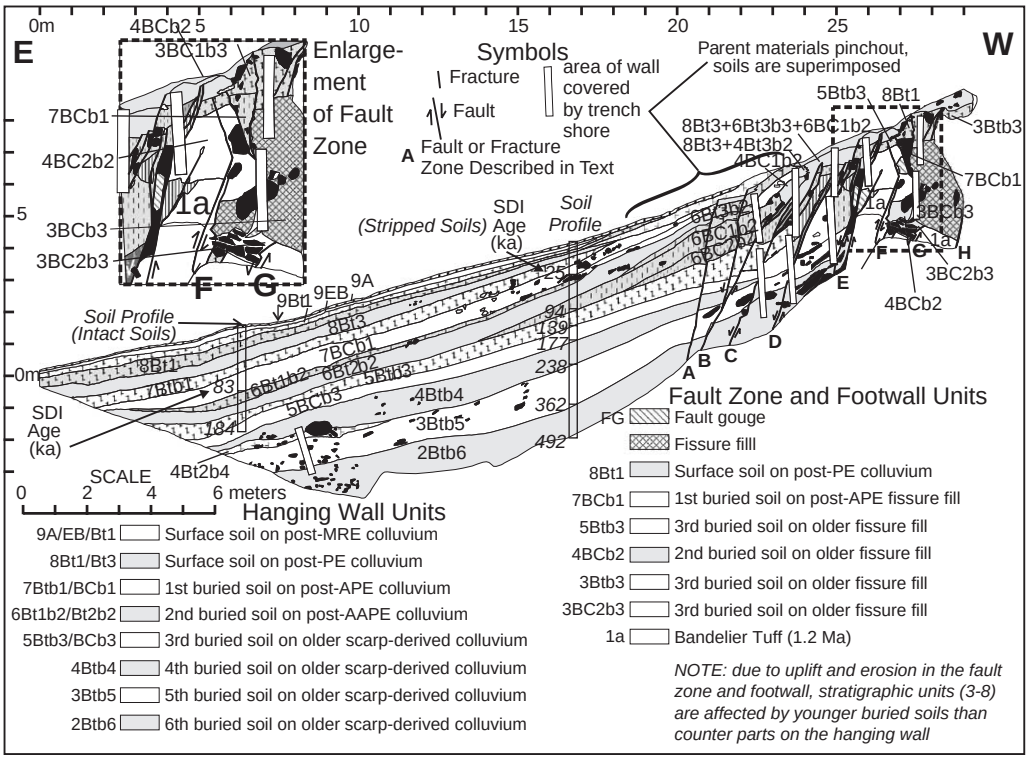

Fig. 8. Log of the south wall of Trench 97-5 across the basal fault zone. Because all map units are soil horizons, I use a mixed scheme of stratigraphic and soil horizon terminology for map units. In this terminology, each unit abbreviation begins with a number that represents a separate soil profile and deposit, with lower numbers representing older deposits (unit 1 is always the Bandelier Tuff, in this and other trench logs). The next letters in the unit abbreviation denote the soil horizon, and lastly, "b1", "b2", etc. indicate buried soils 1 (youngest), buried soil 2, etc. Thus, unit 6Bt2b2 is the sixth soil-colluvial unit from the oldest, the lower part of a two-part textural B horizon (Bt2), and the soil is the second buried soil beneath the ground surface. This same convention is used in all trench logs.

2.2. Graben antithetic scarp (Trenches 97-3, 97-4)

2.2.1. Trench 97-3

Trench 97-3 is located across a 1.5-m-high west-facing fault scarp that bounds the eastern edge of a 200-m-wide graben at the foot of the main Pajarito fault scarp, directly east of Trench 97-5. The trench is 19 m long and up to 5.5 m deep (Fig. 9). Bandelier Tuff is exposed at the surface on the upthrown block, whereas the downthrown block exposes a sequence of fine-grained graben fill sediments strongly over-printed by soil B horizon development.

2.2.1.1. Paleoseismic interpretation. Like Trench 97-5, Trench 97-3 is not dominated by the type of scarp-derived colluvial wedges typical of normal faults elsewhere in the Basin and Range province. Instead, the stratigraphic evidence of paleoearthquakes is a series of nested crack fills on the hanging wall that ascend along the fault plane, and are faulted against a series of paleosols developed on sandy graben sediments. Based on this trench, we propose a generic, conceptual model of how paleoearthquake displacements are recorded on an antithetic scarp where sediment transport is dominantly against the scarp (in this case, from the main scarp to the west). The model assumes repetition of these stages: dip-slip faulting, tectonic fissure creation, fissure filling by scarp-derived debris, scarp burial by graben aggradation equal to the scarp height, and surface stabilization and soil formation (Fig. 10). In Trench 97-3 the three major fissure fills (units 8a, 10, 11 in Fig. 9) are thought to correspond to graben-fill units 12a, 13, and 14, respectively.

Table 1
Thermoluminescence age estimates for Pajarito fault trench studies, Los Alamos National Laboratory New Mexico

Field no.	Lab. sample no.	Stratigraphic unit	Equivalent dose method[a]	Light exposure[b]	Temperature (°C)[c]	Equivalent dose (grays) estimate[d]	TL age (ka)[d]
PF97-2	UIC-635	Colluvium	TL-Total bleach	16 h sun	250–400	494.11 ± 17.54	105.5 ± 10.0
			TL-Total bleach	8 h UV	250–400	503.21 ± 17.63	107.5 ± 10.0
PF97-3	UIC-633	Colluvium	TL-Total bleach	16 h sun	250–350	445.32 ± 15.25	69.5 ± 6.0
			TL-Total bleach	8 h UV	250–350	449.43 ± 15.28	68.5 ± 6.0
PF97-4	UIC-637	Colluvium	TL-Total bleach	16 h sun	250–400	293.61 ± 3.79	94.0 ± 9.0
			TL-Total bleach	8 h UV	250–400	289.94 ± 3.85	93.0 ± 9.0
PF97-5	UIC-634	Colluvium	TL-Total bleach	16 h sun	250–400	206.41 ± 10.31	43.0 ± 4.5
			TL-Total bleach	8 h UV	250–400	206.11 ± 10.41	43.0 ± 4.5
PF97-7	UIC-638	Colluvium	TL-Total bleach reset	thermal (close maximum estimate)	250–350	54.91 ± 6.23	13.0 ± 1.5[e]
PF97-8	UIC-639	Colluvium	TL-Total bleach	thermal reset	250–350 (close maximum estimate)	30.99 ± 3.31	7.0 ± 0.8[e]
PF97-I0	UIC-636	Colluvium	TL-Total bleach	16 h sun	250–350	707.11 ± 32.02	133.0 ± 12.0
			TL-Total bleach	8 h UV	250–350	703.21 ± 31.96	132.0 ± 12.0

[a] All TL measurements were made with a Corning 5/58 and HA-3 filters in front of the photomultiplier tube. Samples were preheated to 124 °C for 48 h prior to analysis.
[b] Hours of light exposure to define residual level. "Sun" is natural sunlight in Chicago, IL. UV is light exposure from 275 W General Electric "sunlamp".
[c] Temperature range used to calculate equivalent dose.
[d] All errors are at 1σ and calculated by averaging the errors across the temperature range. A moisture content of 15 ± 5% was assumed for all samples in the final age calculation.
[e] Preliminary age calculation.

The complex sequence of depositional and faulting events in Trench 97-3 was reconstructed by a 17-step vertical retrodeformation analysis of the trench log (not included herein due to space limitations; see McCalpin, 1998, Fig. 16). The retrodeformation sequence requires 8 displacement events, the first two of which (S_3 and T_3) occurred before the deposition of unit 6. Event U_3 immediately preceded the deposition of colluvial unit 7a, which has an estimated age of ca. 100 ka. All five subsequent events (V_3–Z_3) can be approximately dated by SDI and TL age estimates. Based on the ages and the displacements required by the retrodeformation sequence, we compiled a slip history diagram (Fig. 11). The individual event displacements may be in error by ca. 25% in some cases, but the cumulative vertical displacement must total 7.9 m (distance from the top of the scarp to 5.7 m depth of tuff in the graben, based on a seismic refraction survey of the graben (McCalpin, 1998)). The overall slip rate (7.9 m/1200 ka) is 0.0066 m/ka. In contrast, slip rates during the past ca. 100 ka range from 0.004 to 0.10 m/ka over various seismic cycles (mean = 0.053 m/ka, σ = 0.033 m/ka, COV = 0.62). This degree of slip rate variability through time is slightly less than that deduced for a set of 18 faults in the western USA (McCalpin, 1995). Net vertical displacement per event ranged from 0 (event W_3) to 2.2 m (event T_3), with mean = 0.99 m and σ = 0.67 m, COV = 0.68. This degree of variation is larger than that found by Hecker and Schwartz (1994) in a larger (but currently unpublished) data set where COV was typically <0.3. However, the two data sets mentioned above were collected from primary fault traces, not secondary antithetic faults such as at Trench 3, so a rigorous comparison is not justified.

2.2.2. Trench 97-4

Trench 4 is located across the same west-facing fault scarp as is Trench 3, but 100 m farther south (Fig. 5). The scarp here is only 0.4 m high, compared to the trench depth of up to 3.2 m and length of 14 m. Trench 4 was excavated in hopes of exposing a thicker section of Holocene deposits than was exposed at Trench 3. Holocene deposits were indeed thicker here (55 cm) than at Trench 3 (20–40 cm), and directly overlie a red clayey buried B soil horizon with prismatic ped structure. The two younger Holo-

Table 2
Summary table of radiocarbon dates (all dates on charcoal)

Trench	Unit	Lab. no.	C-14 age	Calendar age[a]	Event constraint
97-3	15b	B-108400	1300 ± 80	1260 (920–1520)	Z3, minimum age
97-4	10c	B-108401	1690 ± 40	1560 (1400–1800)	Z4, minimum age
97-4	10c	B-108402	2230 ± 40	2200, 2310 (2000–2360)	Z4, minimum age
97-7	8a	B-108398	3960 ± 60	4410 (4000–4820)	Z7, close minimum age
97-7	7c	B-108399	4020 ± 50	4450, 4510 (4160–4830)	Z7, close maximum age
97-7	7c	B-113029	1510 ± 50	1360, 1390 (1260–1600)	Z7A, close minimum age
97-7	6	B-113030	2580 ± 40	2740 (2360–2840)	Z7, minimum age
97-7	6	B-113031	2870 ± 40	2960 (2780–3220)	Z7, minimum age
97-7	6	B-113032	2200 ± 50	2150, 2290 (1940–2360)	Z7, minimum age
97-7A	8AC1	B-117083	Modern	N/A	Z7A, far minimum age
97-7A	8D	B-117086	770 ± 50	680 (650–755)	Z7A, far minimum age
97-7A	8Cox2	B-117084	1620 ± 60	1520 (1360–1620)	Z7A, minimum age
97-7A	8Cox3	B-117082	1520 ± 50	1390 (1305–1520)	Z7A, close minimum age
97-7A	8Cox3	B-117085	1450 ± 60	1320 (1270–1420)	Z7A, close minimum age
97-7A	7A?	B-117081	1590 ± 50	1500 (1350–1560)	Z7A, very close maximum age
97-7A	7e	B-117087	1870 ± 70	1815 (1610–1945)	Z7A, close maximum age
97-7A	7b	B-117080	3430 ± 80	3680 (3470–3870)	Z7A, far maximum age
98-4	4c2	B-122086	30,910 ± 180	30,910 ± 180	Y4, maximum age
98-4	4a1	B-122087	29,570 ± 150	29,570 ± 150	Y4, maximum age
98-4	5t1	B-122088	43,660 ± 750	43,660 ± 750	Z4, far maximum age
98-4	1Bw	B-122649	1420 ± 50		Z4, close minimum age
98-4	1cBw	B-122650	840 ± 50		Z4, close minimum age
98-4	3a1	B-122651	17,940 ± 100		Z4, maximum age
98-5	9C	B-122652	400 ± 50		Z5, minimum age

[a] In calibrated years Before Present (cal yr BP), with present taken as 1950 A.D. Calibrated age is the intercept of the mean ^{14}C age with the calibration curve of Stuiver and Reimer (1993). Ages in parentheses are the 2σ limits on the calibrated age.

cene units were in depositional contact with the main normal fault, whereas the oldest Holocene deposit fills in a fissure opened in subjacent red Pleistocene textural B horizon. All pre-Holocene units are in fault contact with Bandelier Tuff (Fig. 12).

2.2.2.1. Paleoseismic interpretation. If our subdivision of fissure fill units is valid, there have been four fissuring events that predate the prominent Pleistocene buried B horizon. However, none of these events can be dated precisely due to the lack of datable material in the coarse-grained fissure fills.

The MRE fractured the red buried B horizon on the south wall of the trench, and dropped pieces of it into a tension fissure on the north trench wall. The presence of tan early Holocene pebbly sand in the fissure, and the undisturbed upper contact of that unit, means either (1) the fissure was still open when the pebbly sand was deposited as crack fill; or (2) the lower part of the pebbly sand had already been deposited atop the Bt horizon as slope wash/alluvium before faulting, it was then down-dropped into the fissure, and slope wash deposition continued. In the first scenario, the event horizon for the MRE is the basal contact of pebbly sand, whereas in the second it is somewhere within the pebbly sand, which is ca. 10 cm thick. ^{14}C ages indicate that the base of the pebbly sand is older than 1.7–2.2 ka, and SDI ages from that contact are 2.3–4.5 ka. Thus, the MRE occurred somewhere after 2.1–4.5 ka, more likely after 2.1–2.3 ka.

2.3. Trench across crestal tension fissure (Trench 97-6)

Trench 97-6 is located on the upper face of the main scarp of the Pajarito fault (Figs. 5 and 6). The lower half of the 7.3-m-deep trench was unknowingly cut through Bandelier Tuff, which was so soft and shattered that it was initially assumed to be fissure fill. Later logging showed that the true fissure fill occupies only the upslope half of the trench (Fig. 13).

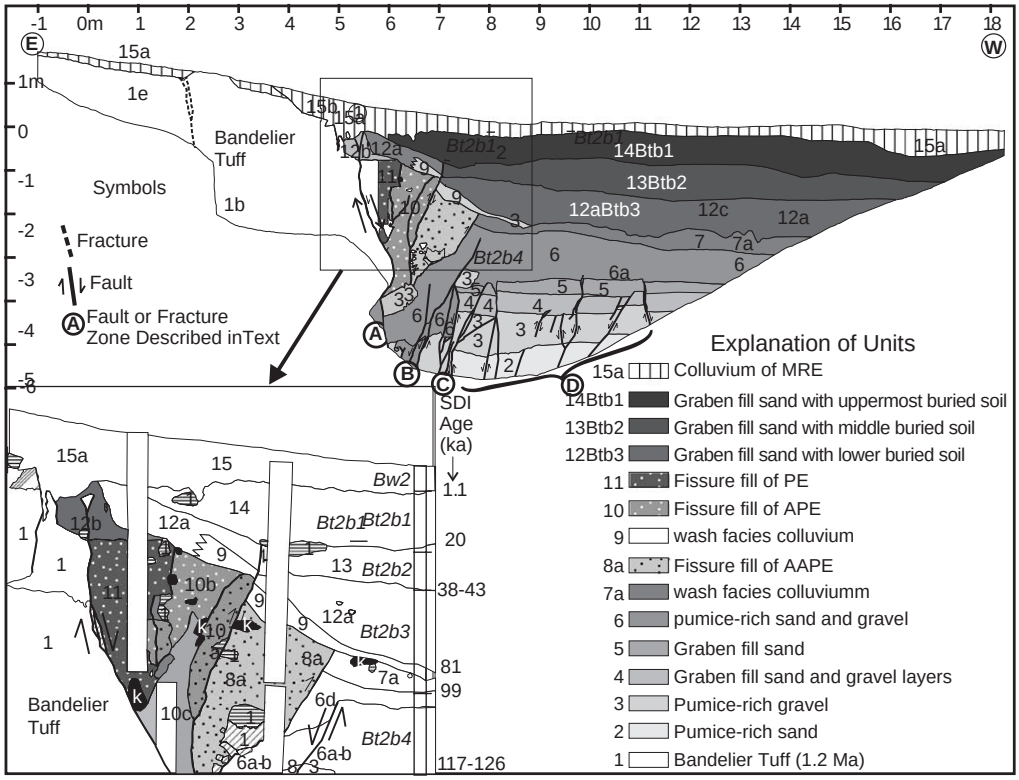

Fig. 9. Log of the south wall of Trench 97-3 across the antithetic scarp on the eastern margin of the 200-m-wide graben. The latest 5 scarp-derived colluvial units are (from youngest to oldest) units 15b and 12a–12b (scarp-derived colluvial wedges), and units 11, 10, and 8 (crack fills); each one is interpreted as evidence for a paleoearthquake displacement. All of these events postdate unit 7, which is TL-dated at 94–106 ka, yielding a long-term recurrence interval of ca. 20 kyr.

2.3.1. Structure

The dominant structures in Trench 97-6 are west-dipping normal faults that displace both Bandelier Tuff and unconsolidated fissure-fill deposits. These faults represent a "domino" style of faulting that affects the entire trench except the westernmost 2 m. Fig. 14 shows a schematic representation of how this domino-style extension works with the concept of a crestal tension fissure. The "back wall" of the crestal tension fissure is the breakaway plane between the stable subhorizontal tuff to the west of the fault scarp, and the east-tilted slab of tuff that comprises the articulated monocline and the scarp face. In our model the back wall maintains its steep (70°–75°) dip throughout all faulting events. With every faulting event the graben at the base of the main fault scarp (below Trench 97-5) drops relatively down, the monoclinal slab of tuff underlying the scarp face tilts incrementally more steeply eastward, and the crestal tension fissure opens by another increment of width. However, if this were the only process acting we would see only a large V-shaped tension fissure in Trench 6 and no other faults.

The pervasive faulting in Trench 97-6 indicates that the upslope end of the east-tilted slab is splintering into separate blocks on a spacing of 0.5–1 m. These blocks accommodate the fault displacement by rotating counterclockwise (viewed to the south, as in Figs. 13 and 14) along their bounding faults, like a series of toppling dominos. This domino-style of faulting has continued to operate as colluvium and crack fill have been deposited here, as evidenced by the domino faults that displace all unconsolidated units (Fig. 13). This rather unique deformation

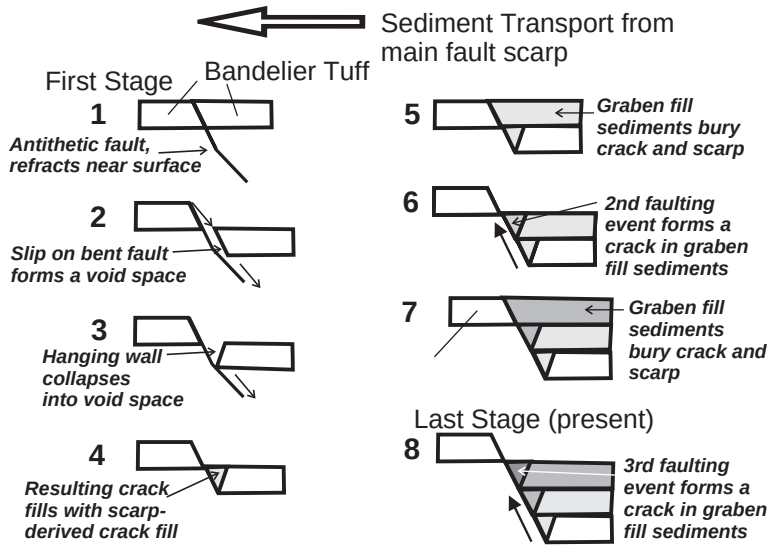

Fig. 10. Schematic cross-sections showing the crack fill-graben aggradation model. Repeated surface rupture exposes a free face composed of bedrock (white), which does not shed appreciable colluvium. Some rock fragments and soil from the free face and upthrown block fall into a tension crack at the base of the scarp, forming a crack fill (Stage 4). Subsequent fluvial deposition fills the graben and buries the scarp face (light gray unit, Stage 5). The next faulting event (Stage 6) drops the graben and creates a second tension crack that cuts the graben sediments. Then the graben aggrades again (medium gray unit, Stage 7). Due to the dip of the fault plane, successively younger crack fills are found up-dip against the fault plane, and the older fills may be rotated (toppled) toward the downthrown block and cut by subsidiary faults, as in Fig. 9.

mechanism creates the unusual situation where down-to-the-east normal faulting at depth is expressed near the surface as a local zone of down-to-the-west faults.

During surface faulting the down-to-the-west domino faults evidently create small scarplets that face upslope on the scarp face. This style of faulting disrupts the normal downslope transport of colluvium on the scarp face, such that colluvial deposits higher on the scarp tend to terminate against these scarplet, instead of continuing to thicken downslope as on a normal fault scarp. For example, the bouldery colluvial wedges of units 10Bt and 9Btb1 in Fig. 13 lie only beneath the upper half of the scarp and pinch out at mid-scarp. This is the opposite geometry to a typical colluvial wedge, which only underlies the lower half of a fault scarp and pinches out at the toe.

2.3.2. Paleoseismic interpretation

The latest two displacement events (Z_6 and Y_6) were followed by the deposition of bouldery scarp-derived colluvial wedges that form distinct stratigraphic units. Each of these events requires movement on the back-wall of the fissure (fault J) to expose fractured tuff in a free face, and domino-style movement on one or more faults to create a backstop to prevent colluvium from being deposited lower on the scarp. A partial retrodeformation sequence (see McCalpin, 1998, Fig. 25) shows that event Z_6 was accompanied by down-to-the west movement of the westernmost fault blocks. Deposition of bouldery colluvium stops at mid-scarp, suggesting that there was a upslope-facing scarplet above fault C. A similar argument can be made for event Y_6, which produced a deep fissure into which colluvial unit 9 was deposited. Unit 9 thickens and becomes considerably coarser grained west of fault D, suggesting that a fault D formed a scarplet that terminated the wedge. Directly underlying this wedge is unit 8, the A horizon of which yielded a TL age of 132 ± 12 ka and an SDI age estimate of 25 ka. Unless we have overlooked evidence for smaller displacement events, there have been only two faulting events post-25 to 132 ka. If each buried soil represents a response to a faulting event, there have been eight faulting events since 1.2 Ma, assuming that there has been no significant erosion of the fissure fill.

Assuming that the fissure record is complete and that each soil formed after a fissuring event, the SDI

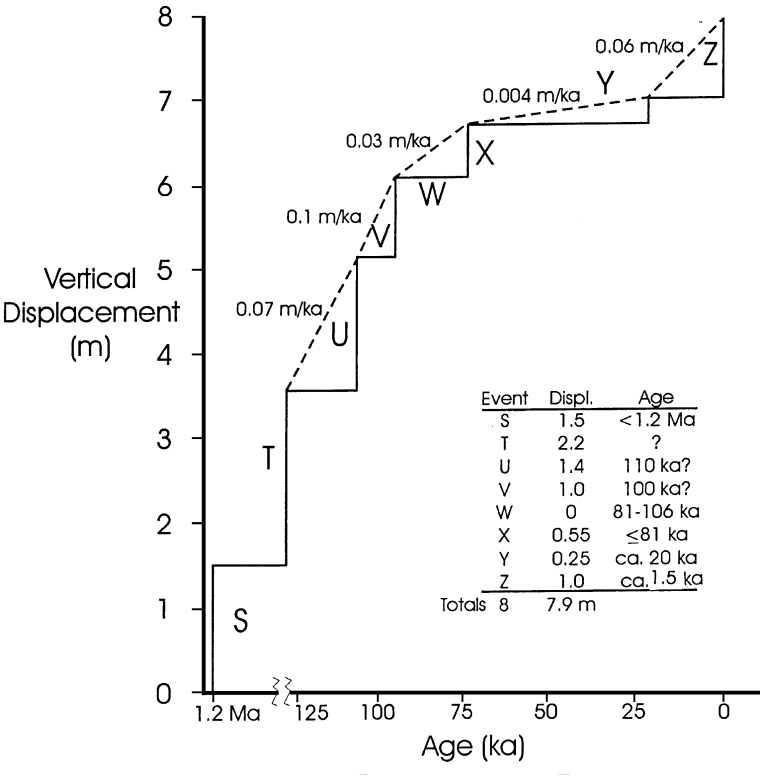

Fig. 11. Slip history diagram for Trench 97-3, based on a detailed retrodeformation sequence. Events V, W, X, Y, and Z are indicated by the youngest two scarp-derived colluvial wedges (units 15b, 12a–b) and the 3 older crack fills (units 11, 10, 8). Events T and U are required by partially preserved distal colluvial wedges (units 7a, 6a–b) in the lowest part of the trench, both of which predate unit 8. Event S is required to create the initial graben at this location, into which units 2–4 (Cerro del Medio pumice and older alluvium) were deposited.

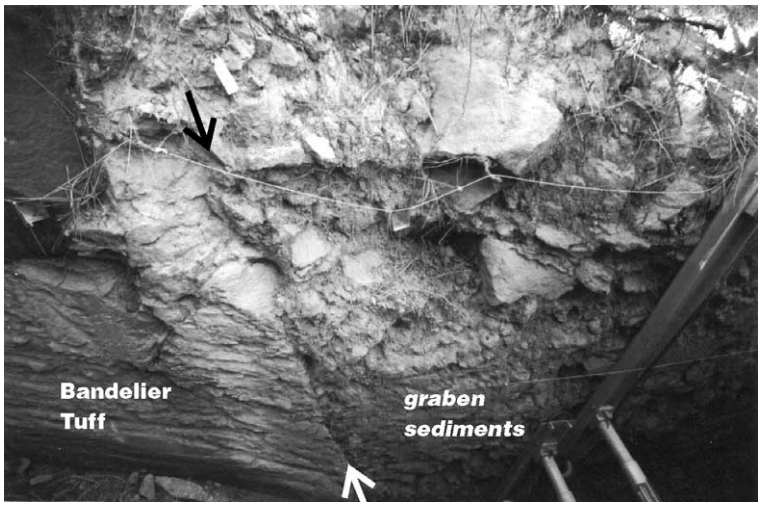

Fig. 12. Photograph of the main fault (between arrows) on the south wall of Trench 97-4, which abuts Bandelier Tuff (left) against late Pleistocene colluvium (right). The stony Holocene alluvium above the upper (black) arrow truncates the fault plane. String lines are about 1 m apart.

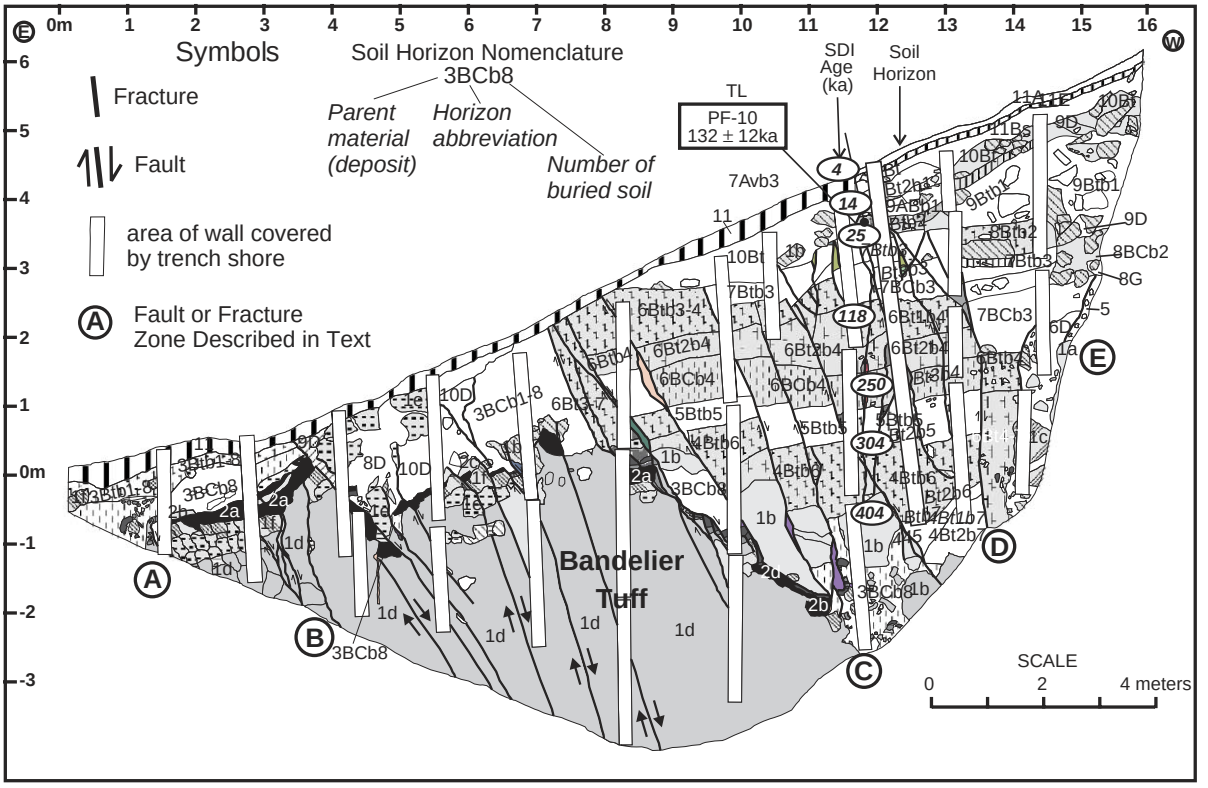

Fig. 13. Log of the south wall of Trench 97-6 in the crestal tension fissure. Both the Bandelier Tuff (all units numbered 1, medium gray) and the sediments deposited in the tension fissure (units 3–11, in alternating white and light gray) are dissected by west-dipping normal faults. These faults develop in passive response to scarp growth and incremental eastward tilting of the articulated monocline. The sediments in the tension fissure are generally clast-poor sands, except units 9 and 10 which contain large angular boulders of Bandelier Tuff derived from a free face coincident with the right wall of the trench (the breakaway plane from intact Bandelier Tuff). All units 3–10 are strongly affected by B horizon soil development, indicating long hiatuses between the deposition of these 8 slope wash units in the tension fissure. These hiatuses may represent interseismic periods, or simply pauses in sedimentation.

ages (from McDonald, 1999) of soil tops are 4, 14, 25, 118, 250, 304, 404, and 445 ka (Fig. 13, circled numbers). If every soil was buried by post-seismic scarp-derived sedimentation, then the 8 ages cited above are approximate paleoearthquake ages.

Our conceptual model for the articulated monocline requires that the crestal tension fissure begin to form as soon as significant vertical displacement accumulates across the fault zone. We do not know exactly when this displacement started, but the results from Trench 97-3 suggest that some faulting predates the 1.1 Ma Cerro del Medio-correlative ash and underlying sediments. Thus, we expect that the basal fissure fill in Trench 97-6 should be on the order of 1 Ma rather than 570 ka and should also have trapped some Cerro del Medio ash, yet the fill clearly does not contain the 1.1 Ma ash or pumice exposed in Trench 97-3. This situation suggests that the graben may have formed very early on this part of the fault zone, before the main scarp accumulated much of its present 50 m height.

2.4. Trenches across antithetic fault on upthrown block (97-7, 97-7A)

2.4.1. Trench 97-7

Trench 97-7 is located on a N–S-trending, west-facing scarp 200 m west of the crest of the main fault scarp (Figs. 5 and 6). This antithetic scarp is quite small (75 cm high), but the 16 m-long, 5-m-deep trench shows a much larger displacement in the subsurface (Fig. 15), as did the other west-facing scarps

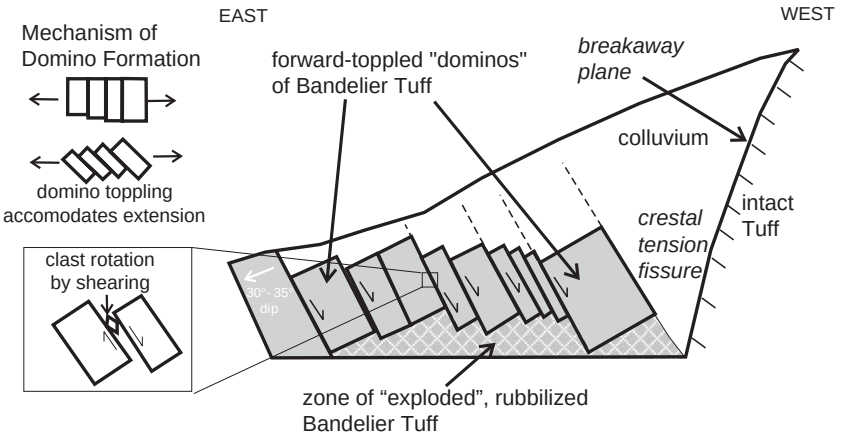

Fig. 14. Schematic structural diagram of Trench 97-6, showing how domino-style faulting affects the downthrown block, down-slope from the colluvium-filled crestal tension fissure. Laminations in the tuff blocks that dip 3°–4° east outside of the fault zone, dip 30°–35° east in the dominos and in the articulated monocline.

trenched (Trenches 97-3, 97-4). Faults in the trench are progressively younger toward the east. Faults in the western half of the trench displace Bandelier Tuff (unit 1), but have only slight or no displacement in the overlying thin ashes (unit 2; probably correlative with the 1.1 Ma Cerro del Medio ash). Fault D in the center of the trench displaces the tuff, ash, and overlying Pleistocene slope wash (units 3,4) and their soil profiles, but does not displace the Holocene alluvium (units 7–9). Between faults A and C is a large tension fissure filled with rubble of two different ages; intact Bandelier Tuff exists east of fault A (i.e., on the footwall). The fissure fills margins do not show any evidence of clast rotation or shearing, suggesting that vertical displacement here was accompanied by a large component of horizontal extension.

2.4.1.1. Paleoseismic interpretation. A minimum of four faulting events are required to reproduce the geometric relations exposed in the trench wall (Fig. 15). These four events are required by faults that terminate upward at different stratigraphic levels, respectively at: (1) the unit 2/3 contact, (2) the unit 3/4 contact, and (3) the two fissure-creating events (units 5b, 6). The latest of these faulting events (Z_7) postdates the lower part of unit 7, if not the entire unit. No movement occurred on faults C or D, but a wide fissured zone was created between faults A and B. The stratigraphic relations suggest that the MRE occurred after the deposition of some or all of the oldest Holocene alluvium, and immediately before the deposition of the colluvial part of unit 7c (contains radiocarbon date 1510 ± 50 yr BP). Thus, the MRE is dated between 1.5 and 4 ka by ^{14}C, or after 7–13 ka by TL and soil development index.

2.4.2. Trench 97-7A

Trench 7A was excavated 1 m south of the eastern part of Trench 7. This small trench (1.8 m deep, 4 m long; Fig. 16) was dug to re-expose the contacts between Holocene alluvium, Bandelier Tuff, and fissure fill that were the sources of some ambiguity in interpreting Trench 7. Trench 7A exposes the same general units exposed in the upper part of Trench 7, i.e. Bandelier Tuff is unit 1, the basal Holocene alluvium is numbered unit 7, somewhat younger Holocene alluvium is numbered unit 8, historic (?) slope wash with no soil formation is numbered unit 9, and the incipient soil developed on the upthrown block is unit 10. Unit 7 has been tilted 15° toward the fault and is truncated at the fault plane by Bandelier Tuff, whereas unit 8 is still horizontally bedded and interfingers with scarp-derived colluvium (units 8D, 8E). Therefore, this shallow trench only exposes evidence for the MRE which occurred after deposition of unit 7 and before deposition of unit 8.

Trench 7A contained small pieces of angular charcoal scattered throughout the stratigraphic section. Radiocarbon dates are generally in correct stratigraphic order, ranging from "modern" (>100% mod-

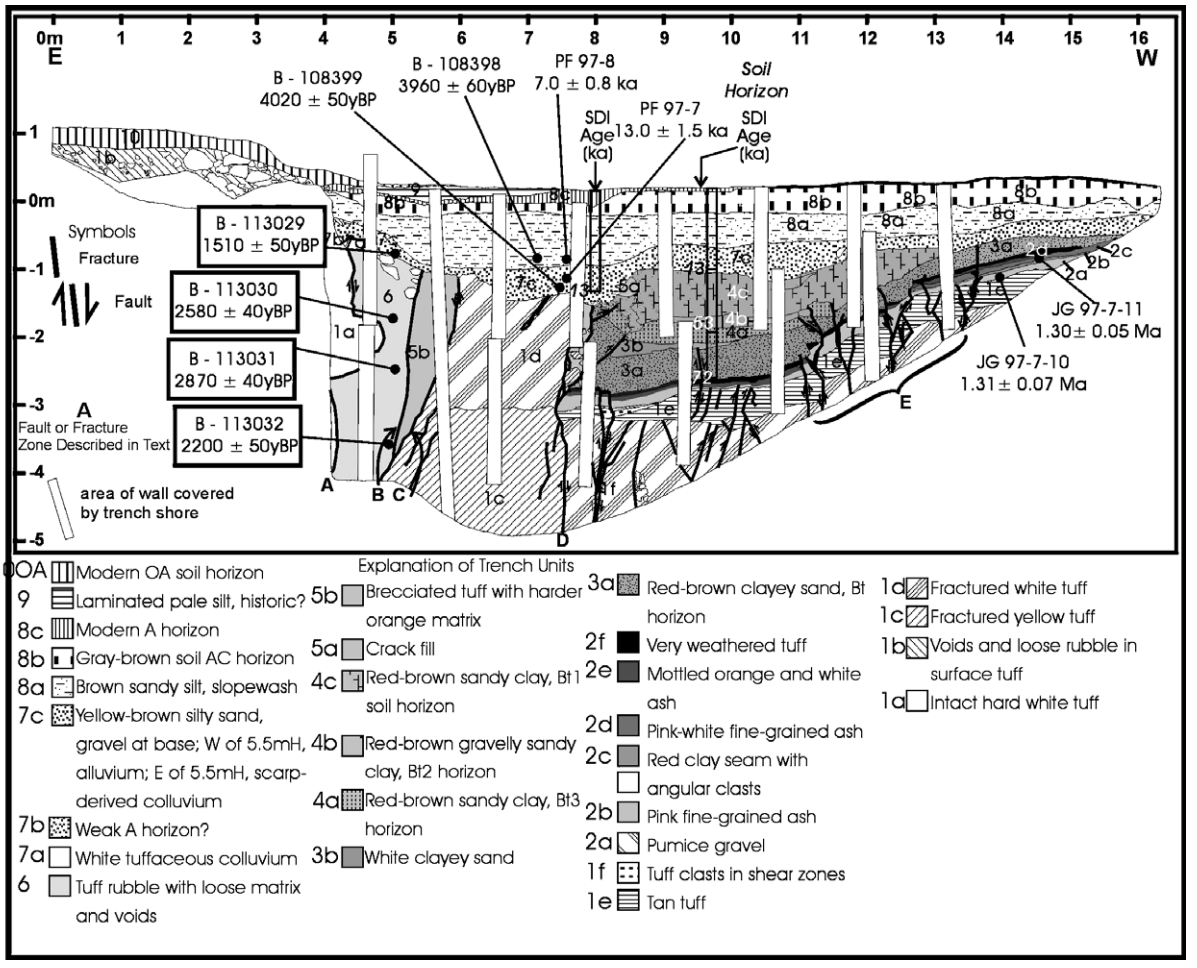

Fig. 15. Log of the south wall of Trench 97-7, across a small antithetic scarp on the upthrown block, west of the crestal tension fissure (see Figs. 5 and 6). Paleoseismic indicators here include two large tension fissures (units 5b, 6) or different age, and upward fault terminations at several stratigraphic levels in the western half of the trench.

ern level of ^{14}C) at 35 cm below the surface to 3430 ± 80 ^{14}C yr BP at 1.2 m below the surface. However, there are some anomalies. The sample from unit 8D, the soft pocket containing clasts, dated at 770 ± 50 ^{14}C yr BP, or 800–900 yrs younger than adjacent soil-stratigraphic units. This large age departure suggest that unit 8D contains intrusive material that is much younger than adjacent strata. Two samples from unit 8Cox3 yielded slightly different ages, 1450 ± 60 and 1520 ± 50 ^{14}C yr BP.

In the tilted part of the stratigraphic section (unit 7) ages are slightly to considerably older than in unit 8. The buried A? horizon (unit 7A) yielded a date of 1590 ± 50 ^{14}C yr BP, which is statistically indistinguishable from the three dates in overlying units 8Cox2 and 8Cox3. Unit 7e dated at 1870 ± 70 ^{14}C yr BP, which does not overlap the cluster of younger dates at 1σ. Finally unit 7b dated at 3430 ± 80 ^{14}C yr BP at a depth of 1.2 m. This compares to a date of 3960 ± 60 ^{14}C yr BP at a depth of 1.05 m in Trench 7.

The MRE in Trench 7A appears to be tightly bracketed by ^{14}C dates at ca. 1500 ^{14}C yr BP. This event timing can be reconciled with that in Trench 7, where unit 7c colluvium shed after the MRE dates at 1510 ± 50 ^{14}C yr BP. This correspondence between the MREs in Trenches 7 and 7A further suggests that the charcoal in the large fissure in Trench 7 (unit 6),

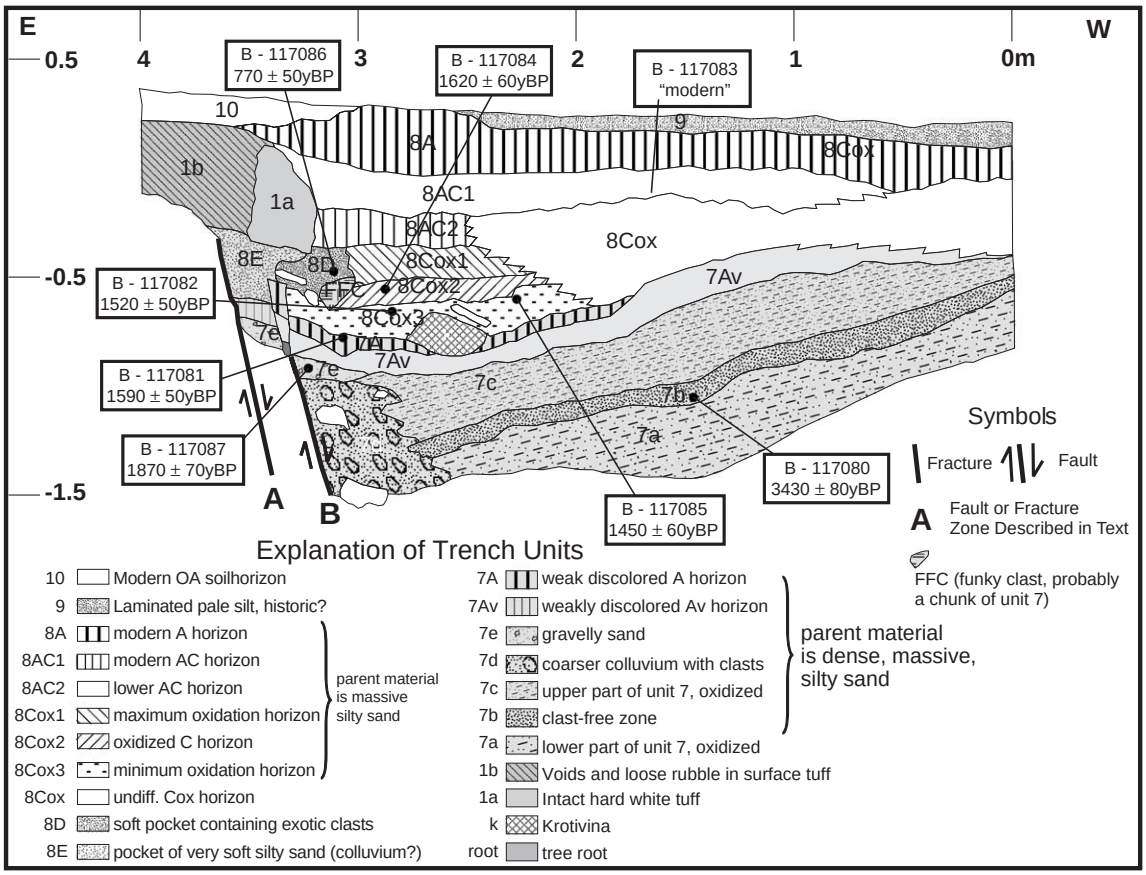

Fig. 16. Log of the south wall of Trench 97-7A. Bandelier Tuff (medium gray shade, units 1a–1b) exists only on the footwall. Two Holocene alluvial units were deposited against the up-slope-facing fault scarp here, the older of which (unit 7) has been tilted toward the fault during the MRE. After tilting of unit 7 and its original soil (7Av), organics accumulated in the depression next to the fault and an organic soil formed (unit 7A). Subsequently a sag pond silt (unit 8Cox3) was deposited. Radiocarbon dates (cited here in ^{14}C years) thus bracket the MRE between about 1590 and 1870 ^{14}C yr BP.

which dated at 2200–2870 ^{14}C yr BP, may be older charcoal washed into open voids.

A related issue is the non-correspondence between young ^{14}C dates and older TL and SDI dates in some trenches. For example, in Trench 7 the lower part of fluvial unit 7c has a ^{14}C age of ca. 4 ka and TL and SDI ages of 13 ka. However, in Trench 4 we have general agreement between ^{14}C dates (1690 ± 40, 2230 ± 40 ^{14}C yr BP) and SDI ages (2.1 ka, 2.3 ka), which are far younger than TL ages (43 ± 5 ka) for the same stratum.

Wong et al. (1995) also experienced discordance between ^{14}C and TL ages in their trenches. At the Water Tanks trenches, pre-El Cajete colluvium yielded ^{14}C dates of $19{,}070 \pm 160$ and $22{,}420 \pm 690$ ^{14}C yr BP, compared to TL ages of 45 ka and 73 ka. Wong et al. (1995, p. 4–39) concluded that the ^{14}C samples were not intrusive into the host deposit, but instead had been contaminated during analysis. They thus explain the two finite dates listed above as resulting from lab contamination of ^{14}C dead charcoal with younger organics.

This explanation cannot be applied to our late Holocene charcoal samples, which all date at less than 4 ka. It would require large amounts of young carbon contamination to yield dates in the range 1.5–4 ka from samples whose true age was 7–13 ka. In addition, it is unlikely that lab contamination would fortuitously result in ^{14}C ages in correct stratigraphic order, as is generally found in Trenches 7 and 7A.

Finally, Beta Analytic periodically runs calibration standards in both its conventional and AMS dating lines, so significant lab contamination would be detected. Therefore, we tend to accept the young radiocarbon ages from Holocene colluvium and alluvium, and consider that much older TL age estimates are due to incomplete initial bleaching of TL at time of deposition. This topic of disagreement between the radiocarbon, luminescence, and soil development methods of dating is discussed at greater length in McCalpin (2000).

2.4.2.1. Paleoseismic interpretation. The sequence of events surrounding the MRE is simple enough that no formal retrodeformation sequence is required. Before the MRE, units 7a–7c were deposited by slope wash against the scarp, and units 7d and 7e were deposited contemporaneously by colluviation. Unit 7b dates at 3430 ± 80 ^{14}C yr BP, and unit 7e at 1870 ± 70 ^{14}C yr BP. Then soil units 7Av and 7A formed atop units 7c and 7e. Unit 7A dates at 1590 ± 50 ^{14}C yr BP.

Later, the MRE occurred displacing unit 7A on fault B (and possibly the lower part of the parent material of 8Cox3) and tilting unit 7 eastward toward the fault. It is most likely that the top of unit 7A was the ground surface at the time of the MRE, and that post-faulting sedimentation on the back-tilted surface began with the parent material of unit 8Cox3. This is the typical response to creating a free face that faces upslope, and creates an event horizon at the top of a buried soil (e.g., see Pantosti et al., 1993).

After the MRE all of unit 8 was deposited and the mapped soil formation developed. For example, unit 8Cox2 dates at 1620 ± 60 ^{14}C yr BP, and the upper part of unit 8Cox3 dates at 1450 ± 60 and 1520 ± 50 ^{14}C yr BP. The lower part of unit 8 was probably deposited more rapidly than soil forming processes, but as deposition rates slowed, soil formation started to keep pace with deposition, yielding the cumulic-style soil with thick AC horizons.

The 15 cm of vertical displacement on the top of unit 7Av? does not represent the entire displacement in the MRE, since additional displacement could have occurred on fault A, the evidence of which is now observed by scarp-derived colluviation. Based on retrodeformation of the Trench 7 wall only 2 m away, the MRE created ca. 1.1 m of vertical displacement.

Thus, the age of the preferred event horizon for the MRE (the 7A/8Cox3 contact) is bracketed by minimum ages of 1450 ± 60 and 1520 ± 50 ^{14}C yr BP, and a maximum age of 1590 ± 50 ^{14}C yr BP.

Based on the dates from Trench 7A, it appears that the MRE occurred about 1500 ^{14}C yr BP, which implies that the unit 7c colluvium in Trench 7 covered the fissure soon after the MRE. However, a fissure formed at 1500 yr BP could not have accepted charcoal inwash between 2200 and 2870 yr BP. Therefore, the 2.2–2.9 ka ^{14}C ages from unit 6 in Trench 7 would be interpreted as very loose minimum age constraints on the penultimate event, rather than constraints on the MRE.

2.5. Trenches across synthetic faults on upthrown block (98-4, 98-5)

In 1998 we excavated six more trenches on the PFZ (McCalpin, 1999), three of which exposed faults and two of which (98-4, 98-5) yielded additional age control on the MRE. Trench 98-4 was excavated across the western splay scarp, a 30-m-high synthetic scarp on the upthrown side of the main PF scarp.

2.5.1. Trench 98-4; Paleoseismic interpretation

Trench 98-4 was excavated across the western splay scarp where it projected across the mouth of an incised drainage. Here the scarp was only 8 m high and displaced the head of a late Pleistocene alluvial fan. The morphology of the scarp was not unusual but the deformation structures beneath the scarp were quite unusual (Fig. 17). Rather than exposing a single, east-dipping normal fault, the trench exposed a complex landslide and thrust fault beneath the center of the scarp, and a highly folded zone beneath the scarp crest. These structures suggest a strong component of east–west compression, despite the fact that this fault forms the margin of a rift zone.

We divided Trench 98-4 into three structural zones. Beneath the toe of the scarp lies the “alluvial fan facies”, composed of undeformed alluvial fan deposits that range from ca. 10 ka to >30 ka. The center of the scarp is underlain by a 10-m-wide rotational slump block, the toe of which merges with a west-dipping thrust fault that extends beneath the trench floor. The deposits in the slump block are a “facies transition

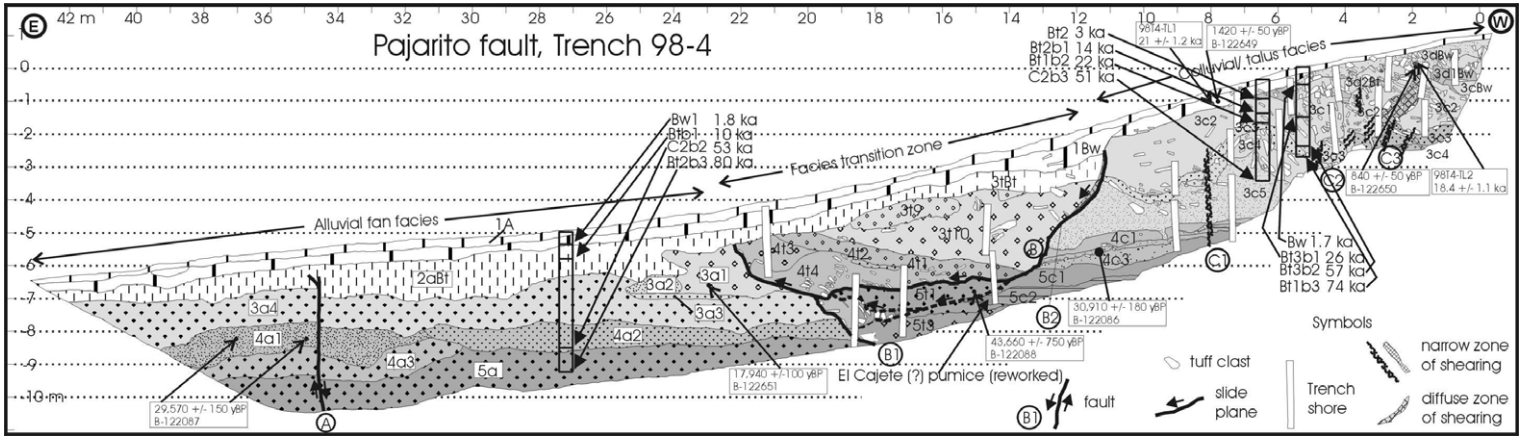

Fig. 17. Log of Trench 98-4. Older deposits are shown in darker gray shades. Three different unit numbering systems are used, for the alluvial fan facies on the hanging wall (unit number followed by an "a"), for facies transition zone in the main deformation area (unit number followed by a "t"), and for the colluvial/talus facies on the footwall (unit number followed by a "c"). Unit numbers 1 through 5 are age-correlative throughout the trench. Radiocarbon dates are in uncalibrated ^{14}C years; B numbers are Beta Analytic, Inc. lab numbers. Soil profile columns show selected soil horizons and the SDI age estimates for those horizons, in ka, from McDonald (1999).

zone" between the fan alluvium to the east and scarp-derived colluvium to the west. For example, units 3t9 and 3t10 that comprise the upper part of the slump block are colluvial equivalents to the middle alluvial fan unit (unit 3a). Subjacent units 4t and 5t in the slump block are correlative to alluvial strata to the east, over which they have been thrust. The scarp crest is underlain by a "colluvial/talus facies" composed of large angular blocks of Bandelier Tuff (unit 3) that overlies better-stratified alluvial units (4c, 5c). All units beneath the scarp crest are folded into open, north-trending folds with wavelengths of 2–4 m and amplitudes of ca. 1 m. The author has never observed such fold structures in normal fault exposures elsewhere.

The deformation exposed in Trench 98-4 affects all units except the surface soil A and Bw horizons at the scarp crest, the latter of which contains charcoal dated at 1.4–1.8 ka. The steep clast orientations in unit 3cBw beneath the scarp crest suggest that unit has been folded and rotated by deformation, but this evidence is rather indirect. In the "alluvial fan facies" the base of unit 2aBt is offset, but not the top of the unit. The base of the unit 2a debris flow may be tectonically offset, or the debris flow may be draped over a small scarp in the top of unit 3a4. Thus all we know with certainty is that unit 3a4 is offset, but buried soil 1 is not offset. This brackets offset on this small antithetic fault between about 10 ka (age of unfaulted buried soil 1) and 17.9 ka (age of faulted unit 3a4).

At the head of the "facies transitional zone", soil 3tBt appears to be truncated at the headscarp of the rotational slump, but actually the parent material unit 3 colluvium is truncated, not the pedogenic horizon. The Bt soil horizon continues westward into unit 3c2, so displacement on this structure predates formation of buried soil 1 [variously dated by PDI at 10 ka (27.2 mH), 14 ka (6.5 mH), and 26 ka (5.4 mH)], and post-dates unit 3t, which is undated.

At the head of the trench at least three episodes of deformation are indicated. The oldest is compressional deformation needed to fold units 3c2–3c5 and to rotate their clasts to their present steep dips. The second is extensional deformation that dismembered unit 3c3 and opened the fissure into which unit 3c1 was deposited. The steep dips of clasts in units 3cBt and 3cBw appear to require a third episode of penetrative deformation.

Notably, at the head of the trench we observe young soils developed on old deformed parent materials that were brought up to the surface by folding and then erosionally truncated. This distinction between old parent materials and younger soils emphasizes a danger in using either soil SDI values or radiocarbon dates on charcoal to estimate deposit ages beneath the upper half of a fault scarp. In the first case, SDI values only tell us the amount of soil development time, not the age of the parent material on which the soils are developed. In depositional environments such as an alluvial fan or a scarp-derived colluvial wedge, deposits are laid down quickly and then soil development proceeds on them, so soil SDI ages can closely approximate deposit age. This approximation works because elapsed geologic time is composed only of deposition time (negligible to short) and soil development time. In contrast, at the crest of this fault scarp geologic time has been composed of deposition time, folding time, erosion time, and soil development time. Soil SDI values only permit estimation of the last component.

In the second case, young charcoal can become introduced into the young soils developed on old deposits at the scarp crest. Two pairs of TL and ^{14}C ages at the head of the trench illustrate this problem. At meter 8 on the log, the soil overlying unit 3c2 yielded a ^{14}C age on charcoal of 1420 ± 50 ^{14}C yr BP and an adjacent TL age estimate of 21 ± 1.2 ka. At meter 2 on the log, unit 3dBw yielded a ^{14}C age on charcoal of 840 ± 50 ^{14}C yr BP and an adjacent TL age estimate of 18.4 ± 1.1 ka. The TL ages are similar to the SDI age estimates for this soil (14–26 ka) and are probably relatively accurate age estimates for the eroded deposits beneath the scarp crest, whereas the charcoal is much younger and was introduced in the very late Holocene during a period of soil development.

Given the distinctions outlined above, the folded deposits at the head of the trench are definitely younger than the El Cajete pumice (50–60 ka), perhaps 18–21 ka by TL and 14–26 ka by SDI, and are much older than soil 1 dated at 1420 ^{14}C yr BP. The folding must be older than the soils developed in units above the folds, i.e. buried soil 1, which is dated in units by PDI at 14–26 ka. However, these ages are only minimum ages for the folded deposits.

The episode of extensional deformation at the trench head can be indirectly dated by soil SDI. Horizon Bt2b1 at 6.5 m from the head of the trench covers the crack fill of unit 3c1 and must post-date the crack, and dates at ca. 14 ka. Horizon Bt3b1 at 5.4 m from the head of the trench carries an older SDI age (26 ka), but this horizon is developed on the crack fill, and the crack fill parent material is unit 3 which already carried a soil before crack formation. Thus, I believe that the SDI age of 26 ka for unit 3c1 overestimates its age, because that unit is composed of "recycled" pieces of preexisting Bt horizons from either side of the fissure. If the crack fill formed before 14 ka, and well after 26 ka, then its time range overlaps the time range of antithetic faulting and rotational slumping farther downslope in the trench (10–17.9 ka). Thus, it is possible that all the extensional deformation in the trench occurred at the same time, ca. 10–18 ka.

3. Conclusions

3.1. Refinement of the structural model of the Pajarito fault

The structural model of the PF (articulated monocline) was originally based on surface observations (McCalpin, 1997) plus limited subsurface exposures such as the Wong et al. (1993) trenches and road-cuts along NM Highway 4. Our eight trenches excavated in 1997 provide additional subsurface information that bears on this model. The main uncertainty about structure in monoclinal sections of the scarp is where the underlying normal fault is located with respect to the east-tilted slab. It will not be possible to determine this geometry without a prohibitively expensive drilling program, and such detailed knowledge of subsurface fault geometry really does not contribute much critical information to the seismic hazard analysis.

3.2. Timing of the most recent faulting event

A Holocene faulting event is required by the mapped stratigraphic relationships exposed in Trenches 97-3, 97-4, 97-7, 97-7A, 98-4 and 98-5, with suggestive evidence in Trenches 97-2 and 97-5. The timing of the MRE is mainly constrained by ^{14}C dates (Table 2), with a few SDI ages also relevant. In general, TL and SDI age estimates from within 1 m or less from the ground surface are much older than ^{14}C ages, for reasons explained previously. The limiting ages for the MREs are shown graphically in Fig. 18.

The age estimates that constrain the MRE from 1997 trenches are mainly radiocarbon ages from post-faulting colluvial deposits on the hanging wall, whereas constraining ages from the 1998 trenches are mainly radiocarbon ages from young soils developed on older (pre-faulting) deposits on the footwall. Because of this difference in stratigraphic position, the 1998 ages (range 10–20 ka, overlap 13–18 ka) tend to be older as a group than the 1997 ages (range 2–16 ka, overlap 3–11 ka). However, based on their similar stratigraphic setting, we conclude that these MREs are actually the same event, and that the apparent difference in radiocarbon limiting ages results from the different stratigraphic settings.

3.3. Recurrence intervals between paleoearthquakes on the Pajarito fault

As displayed in the retrodeformation sequences for Trenches 97-3 and 97-7, we can roughly estimate the length of time intervals between paleoearthquakes that predate the MRE. In Trench 97-3 we have evidence for six events (five recurrence intervals) in the period from 1.5 ka to ca. 110 ka, which yields a long-term mean recurrence of 21.7 ka. However, recurrence is extremely variable, ranging from <10 ka to ca. 61 ka. The standard deviation of the recurrence series is 20.1 ka, which defines a coefficient of variation (COV, σ/mean) of 0.95. This high degree of variability is rarely found in paleoseismic recurrence series elsewhere (McCalpin and Slemmons, 1998), and suggests that either: (1) the dating of events here is inaccurate; (2) there are missing events in the series; or (3) not all earthquakes on the Pajarito fault are recorded in Trench 97-3. The three latest events in Trench 97-7 in the past 72 ka have a mean recurrence of 34 ka, σ of 15 ka, and COV of 0.44. This COV is more typical of paleoearthquake sequences elsewhere, although Trench 97-7, being far west of the main fault scarp, is even less likely than Trench 3 to record all the surface-rupturing earthquake that have occurred on the Pajarito fault.

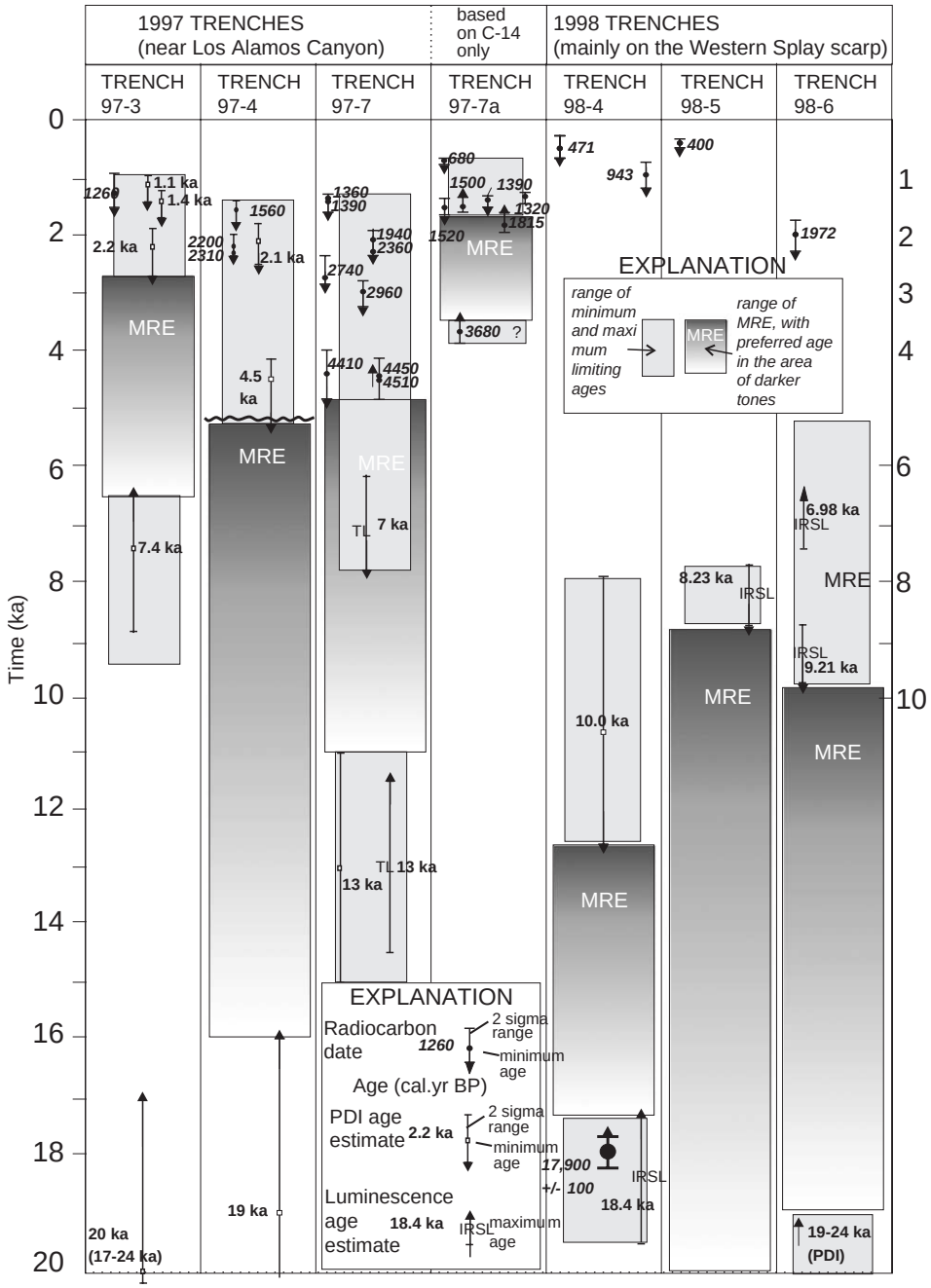

Fig. 18. Space–time diagram showing the limiting ages on the MREs in the 1997 and 1998 trenches. The inferred time span for each event is shown by the shaded boxes, with the preferred age range shown by the darker shade in each box. Stratigraphic evidence from the trenches indicates only a single Holocene paleoearthquake, so I conclude that the MRE in the 1997 and 1998 trenches is actually the same event. The apparent difference in bracketing ages for the MRE in the 1997 and 1998 trenches is attributed to different dating techniques used in those 2 years, as explained in the text.

In Trenches 97-5 and 97-6 event horizons are insufficiently preserved to identify and date paleoearthquakes with confidence. Repeated episodes of colluvial deposition and subsequent soil formation can be definitely related to earthquake displacements in some, but not all cases. If we assume that most depositional episodes in our tectonic depressions are related to faulting, we can analyze the durations of soil-forming between these episodes as if they were recurrence intervals. In the center of Trench 97-5 soil ages are 25, 91, 139, 177, 238, 362, and 492 ka, yielding soil durations of 66, 48, 38, 61, 124, and 130 ka. This series has a mean of 77.8 ka, σ of 35.9 ka, and COV of 0.46.

In Trench 97-6 soil ages are 4, 14, 25, 118, 250, 304, 404, and 445 ka, yielding soil durations of 10, 11, 93, 132, 54, 100, and 41 ka. This series has a mean of 63 ka, σ of 43.3 ka, and COV of 0.69. It is interesting that the calculated recurrence intervals in the past 100 ka from the two small antithetic faults (Trench 3, 21 ka; Trench 7, 34 ka) are much shorter than the post-500 ka recurrence intervals from the two trenches on the main fault scarp (Trench 97-5, 78 ka; Trench 97-6, 63 ka). One would expect that a higher proportion of the total post-500 ka faulting events on the Pajarito fault would be recorded on the main fault trace, rather than on smaller antithetic faults. It seems reasonable that the main-scarp faults exposed in Trenches 97-5 and 97-6 have moved at least as many times as those in Trenches 3 and 7. Thus, my interpretation of the apparent longer recurrence times in Trenches 97-5 and 97-6 is that many faulting events occurred on those faults which we could not detect during logging, due mainly to the heavy overprinting of homogeneous colluvium with strong textural B horizons.

Acknowledgments

This study would not have been possible without the support and cooperation of LANL personnel, in particular Douglas E. Volkman, Jamie N. Gardner, and Steven L. Reneau. Alexis Lavine also assisted in trench cleaning, logging and surveying. Our trenching crew of Margaret E. Berry, Molly Bentley, Jason Amato, Tom Cooper, Al Jones, and Juan-Carlos Moya persevered through rain, snow, hail, sleet, and mud to produce some fine trench logs. Eric McDonald described soils in our trenches and Steve Forman collected and analyzed luminescence samples, as well as assisting with trench interpretation. Trench reviewers William R. Lettis and Frank H. Swan provided many helpful observations during their field review. Susan S. Olig and Ivan G. Wong contributed information on the previous trenching by Woodward-Clyde Federal Services. Our day-to-day trench safety was ensured by Mr. Ron Riggins (Johnson Controls, Inc.). We also thank the efficient crew from Parker Construction for their artful trench shoring, particularly Mr. Brad Parker. Early versions of this report benefitted from technical reviews by F.H. Swan, W.R. Lettis, J.N. Gardner, and A. Lavine. The manuscript was critically reviewed by M.N. Machette, F. Audemard, and A. Michetti.

References

Aldrich, M.J., Dethier, D.P., 1990. Stratigraphic and tectonic evolution of the northern Española Basin, Rio Grande rift, New Mexico. Geological Society of America Bulletin 102, 1695–1705.

Bailey, R.A., Smith, R.L., Ross, C.S., 1969. Stratigraphic nomenclature of volcanic rocks in the Jemez Mountains, New Mexico. U.S. Geological Survey Bulletin 1274-P. 19 pp.

Gardner, J.N., Goff, F., Garcia, S., Hagan, R.C., 1986. Stratigraphic relations and lithologic variations in the Jemez volcanic field, New Mexico. Journal of Geophysical Research 91, 1763–1778.

Gardner, J.N., Baldridge, W.S., Gribble, R., Manley, K., Tanaka, K., Geissman, J.W., Gonzalez, M., Baron, G., 1990. Results from seismic hazards trench #1 (SHT-1). Los Alamos Seismic Hazards Investigations: Los Alamos National Laboratory Report EES1-SH90-19. 57 pp.

Harden, J.W., 1982. A quantitative index of soil development from field descriptions—examples from a chronosequence in central California. Geoderma 28, 1–28.

Harden, J.W., Taylor, E.M., 1983. A quantitative comparison of soil development in four climatic regimes. Quaternary Research 20, 342–359.

Hecker, S., Schwartz, D.P., 1994. The characteristic earthquake revisited; geological evidence of the size and location of successive earthquakes on large faults. Open-File Report (U.S. Geological Survey) 94-568, 79–80.

Kelley, V.C., 1978. Geology of the Española Basin, New Mexico: New Mexico Bureau of Mines and Mineral Resources, Geologic Map 48, scale 1:125,000.

Kelson, K.I., Hemphill-Haley, M.A., Olig, S.S., Simpson, G.D., Gardner, J.N., Reneau, S.L., Kolbe, T.K., Forman, S.L., Wong, I.G., 1996. Late Pleistocene and possibly Holocene

displacement along the Rendija Canyon fault, Los Alamos County, New Mexico. New Mexico Geological Society Guidebook, 47th Field Conference, Jemez Mountains Region.

McCalpin, J.P., 1995. Frequency distribution of geologically-determined slip rates for normal faults in the western USA. Bulletin of the Seismological Society of America 85 (6), 1867–1872.

McCalpin, J.P. (Ed.), 1996. Paleoseismology. Academic Press, New York. 583 pp.

McCalpin, J.P., 1997. Geomorphology and structure of the Pajarito fault zone west of Los Alamos National Laboratory, New Mexico: unpublished report submitted to Los Alamos National Laboratory, Los Alamos, NM, by GEO-HAZ Consulting, Inc., Estes Park, CO, April 9, 1997, 54 plus 12 oversized maps at 1:1200 scale.

McCalpin, J.P., 1998. Late Quaternary faulting on the Pajarito fault, west of Los Alamos National Laboratory, north-central New Mexico. Results from the seven-trench transect excavated in summer of 1997: unpublished report submitted to Los Alamos National Laboratory, Los Alamos, NM by GEO-HAZ Consulting, Inc., Estes Park, CO, May 9, 1998. 105 plus appendices.

McCalpin, J.P., 1999. Late Quaternary faulting on the Pajarito fault, west of Los Alamos National Laboratory, north-central New Mexico. Results from seven trenches excavated in summer of 1998. Final Report: LANL report LA-UR-99-1120, submitted to Los Alamos National Laboratory. Los Alamos, NM by GEO-HAZ Consulting, Inc., Estes Park, CO, Aug. 31, 1998. 104 pp.

McCalpin, J.P., 2000. Late Quaternary faulting on the Pajarito fault, west of Los Alamos National Laboratory, north-central New Mexico. Summary Chronology of Quaternary Faulting Events; unpublished report submitted to Los Alamos National Laboratory. Los Alamos, New Mexico by GEO-HAZ Consulting, Inc., Estes Park, Colorado, April 10, 2000. 23 pp.

McCalpin, J.P., Slemmons, D.B., 1998. Statistics of paleoseismic data: unpublished Final Technical Report submitted to U.S. Geological Survey, Reston, VA by GEO-HAZ Consulting, Inc., Estes Park, CO. Contract 1434-HQ-96-GR-02752, March 20, 1998. 62 pp.

McDonald, E., 1999. LANL seismic hazard trench investigations. Soil stratigraphy and pedologic age estimates for late Quaternary faulting on the Pajarito fault, west of Los Alamos National Laboratory. Results from 1997 and 1998 trench excavations: unpublished final report submitted to Los Alamos National Laboratory by Eric McDonald, Desert Research Institute, Reno, NV, Feb. 1999. 82 plus figures and appendices.

Olig, S.S., Kelson, K.I., Gardner, J.N., Reneau, S.L., Hemphill-Haley, M.A., 1996. The earthquake potential of the Pajarito fault system, New Mexico. New Mexico Geological Society Guidebook, 47th Field Conference, Jemez Mountains, pp. 143–152.

Pantosti, D., Schwartz, D.P., Valensise, G., 1993. Paleoseismology along the 1980 surface rupture of the Irpina fault; implications for earthquake recurrence in the southern Appennines, Italy. Journal of Geophysical Research 98, 6561–6577.

Powell, J.W., 1873. Geological structure of a district of country lying to the north of the Grand Canyon of the Colorado. American Journal of Science 5, 456–465.

Smith, R.L., Bailey, R.A., 1966. The Bandelier Tuff; a study of ash-flow eruption cycles and zoned magma chambers. Bulletin Volcanologique 29, 83–104.

Smith, R.L., Bailey, R.A., Ross, C.S., 1970. Geologic map of the Jemez Mountains. New Mexico: U.S. Geological Survey, Miscellaneous Investigations Map I-571, scale 1:125,000.

Stuiver, M., Reimer, P.J., 1993. Extended ^{14}C data base and revised CALIB 3.0 ^{14}C age calibration program. Radiocarbon 35, 215–230.

Taylor, E.M., 1988. Instructions for the soil development index template—Lotus 1-2-3. Open-File Report U.S. Geological Survey, vol. 233A.

Wong, I. et al., 1993. Seismic hazards evaluation of the Los Alamos National Laboratory, Draft Final Report: submitted to Los Alamos National Laboratory by Woodward Clyde Federal Services, June 1, 1993. 3 vols.

Wong, I. et al., 1995. Seismic hazards evaluation of the Los Alamos National Laboratory, Final Report: submitted to Los Alamos National Laboratory by Woodward Clyde Federal Services, 25 Feb. 1995. 3 vols.